



# Dragging 3D printing technique controls pore sizes of tissue engineered blood vessels to induce spontaneous cellular assembly

Hun-Jin Jeong<sup>a,g,1</sup>, Hyoryung Nam<sup>b,1</sup>, Jae-Seok Kim<sup>a</sup>, Sungkeon Cho<sup>d</sup>, Hyun-Ha Park<sup>a</sup>, Young-Sam Cho<sup>c</sup>, Hyungkook Jeon<sup>h</sup>, Jinah Jang<sup>b,d,e,f,\*</sup>, Seung-Jae Lee<sup>c,\*\*</sup>

<sup>a</sup> Department of Mechanical Engineering, Wonkwang University, 54538, Iksan, Republic of Korea

<sup>b</sup> Department of Convergence IT Engineering, Pohang University of Science and Technology, 37673, Pohang, Gyeongbuk, Republic of Korea

<sup>c</sup> Department of Mechanical and Design Engineering, Wonkwang University, 54538, Iksan, Republic of Korea

<sup>d</sup> Department of Mechanical Engineering, Pohang University of Science and Technology, 37673, Pohang, Gyeongbuk, Republic of Korea

<sup>e</sup> School of Interdisciplinary Bioscience and Bioengineering, Pohang University of Science and Technology, 37673, Pohang, Gyeongbuk, Republic of Korea

<sup>f</sup> Institute of Convergence Science, Yonsei University, 03722, Seoul, Republic of Korea

<sup>g</sup> Regenerative Engineering Laboratory, Columbia University, 630W 168th ST, New York, 10032, USA

<sup>h</sup> Department of Manufacturing Systems and Design Engineering, Seoul National University of Science and Technology, 01811, Seoul, Republic of Korea

## ARTICLE INFO

### Keywords:

Small diameter vessel

Dragging 3D printing

Pore control

Spontaneous cellular assembly

## ABSTRACT

To date, several off-the-shelf products such as artificial blood vessel grafts have been reported and clinically tested for small diameter vessel (SDV) replacement. However, conventional artificial blood vessel grafts lack endothelium and, thus, are not ideal for SDV transplantation as they can cause thrombosis. In addition, a successful artificial blood vessel graft for SDV must have sufficient mechanical properties to withstand various external stresses. Here, we developed a spontaneous cellular assembly SDV (S-SDV) that develops without additional intervention. By improving the dragging 3D printing technique, SDV constructs with free-form, multilayers and controllable pore size can be fabricated at once. Then, The S-SDV filled in the natural polymer bioink containing human umbilical vein endothelial cells (HUVECs) and human aorta smooth muscle cells (HAoSMCs). The endothelium can be induced by migration and self-assembly of endothelial cells through pores of the SDV construct. The antiplatelet adhesion of the formed endothelium on the luminal surface was also confirmed. In addition, this S-SDV had sufficient mechanical properties (burst pressure, suture retention, leakage test) for transplantation. We believe that the S-SDV could address the challenges of conventional SDVs: notably, endothelial formation and mechanical properties. In particular, the S-SDV can be designed simply as a free-form structure with a desired pore size. Since endothelial formation through the pore is easy even in free-form constructs, it is expected to be useful for endothelial formation in vascular structures with branch or curve shapes, and in other tubular tissues such as the esophagus.

## 1. Introduction

Cardiovascular disease (CVD), a complex group of disorders that includes peripheral arterial disease (PAD), coronary artery disease (CAD), cerebrovascular disease, and aortic atherosclerosis, is the leading cause of death worldwide from non-communicable diseases [1,2]. CVD caused about 19.1 million deaths in 2020, and the annual mortality rate

is estimated to increase to 23 million by 2030 [3]. When ischemic heart disease occurs due to atherosclerosis or coronary artery disease, the coronary arteries are narrowed or blocked [4]. This can lead to serious organ damage such as angina pectoris or myocardial infarction, and sudden death due to lack of sufficient blood and oxygen supplied to the myocardium [3]. Coronary artery bypass graft (CABG) is the most common surgical method to solve this problem. It is estimated that over

Peer review under responsibility of KeAi Communications Co., Ltd.

\* Corresponding author. Department of Convergence IT Engineering, Pohang University of Science and Technology, 37673, Pohang, Gyeongbuk, Republic of Korea.

\*\* Corresponding author. Department of Mechanical and Design Engineering, Wonkwang University, 54538, Iksan, Republic of Korea.

E-mail addresses: [jinahjang@postech.ac.kr](mailto:jinahjang@postech.ac.kr) (J. Jang), [sjlee411@wku.ac.kr](mailto:sjlee411@wku.ac.kr) (S.-J. Lee).

<sup>1</sup> These authors contributed equally to this work.

<https://doi.org/10.1016/j.bioactmat.2023.07.021>

Received 9 February 2023; Received in revised form 23 June 2023; Accepted 24 July 2023

Available online 4 October 2023

2452-199X/© 2023 The Authors. Publishing services by Elsevier B.V. on behalf of KeAi Communications Co. Ltd. This is an open access article under the CC BY-NC-ND license (<http://creativecommons.org/licenses/by-nc-nd/4.0/>).

500,000 CABG procedures are performed in the United States annually. Most CABG procedures use autologous blood vessels, and the patency rate is very high at 90% after 1 year of the transplantation [4,5]. A challenge to this procedure is that it is difficult to find suitable autologous blood vessels. Moreover, it is estimated that over 30% of CVD patients do not have adequate blood vessels. Even if an autologous blood vessel is obtained, the length or diameter may not be sufficient. Additionally, if secondary bypass surgery is performed, the possibility of finding another suitable autologous vessel is significantly reduced. The autologous blood vessel is obtained by invasive sampling, which provides an additional surgical scar. If the autologous blood vessel wall gets damaged during the collection process, other chronic diseases or wound complications are added, which can cause morbidity at the donor site [6–8].

Accordingly, artificial blood vessel grafts to replace autologous blood vessels are being manufactured in the field of tissue engineering [9–12]. Due to the high clinical demand for artificial blood vessel grafts, several off-the-shelf products have been developed using synthetic polymers (e.g., polyethylene terephthalate (Dacron) and polytetrafluoroethylene (Teflon) and ePTFE (GORE-TEX)) [13–16]. These artificial blood vessel grafts have been able to successfully replace diseased vessels when transplanting medium or large diameter blood vessels [15–17]. However, CABG, which requires transplantation of small diameter vessels with an inner diameter of less than 5 mm, has shown disappointing clinical results, due to blood clots caused by damaged or dysfunctional endothelium. The off-the-shelf artificial blood vessels do not have endothelium. In the case of medium or large diameter grafts, blood flow is high even without endothelium, so there is less chance of clot formation. However, in case of small diameter vascular (typically less than 5 mm inner diameter) are plagued that thrombosis and thickening of the neointimal as well-known as intimal hyperplasia. To overcome these limitations, it is essential to form an endothelial cell layer inside the artificial SDV [18,19].

Numerous manufacturing technologies are being actively researched to produce tubular SDVs with endothelium in the inner layer [12, 20–22]. The tubular construct of blood vessels requires a high level of processing skill due to the complex hierarchical construct that includes a variety of cell types and ECMs. Conventional fabrication techniques have been extensively studied to fabricate multilayer tubular constructs

containing endothelium (e.g., electrospinning, cell sheet engineering, and mold casting). However, manufacturing 3D tubular constructs requires a long time and is a labor-intensive multi-step process, limiting production. 3D bioprinting technology has emerged as an effective approach to overcome these limitations. Using this method, the tubular SDV can be fabricated quickly and easily [2,23–29]. Cell-laden tubular construct in a natural polymer that helps cells grow also can be manufactured. However, mostly it has weak mechanical properties, making it difficult to use in clinics [11]. We developed a dragging printing technique using 3D printing as described in a previous study. Through this, we produced a tubular artificial esophagus construct in which esophageal epithelial cells and esophageal smooth muscle cells were evenly laden with natural polymers that helped the cells grow [2]. The fabricated esophageal construct had sufficient mechanical properties to be used in clinics. During the research, it was confirmed that the presence of pores helped not only the mechanical properties of the construct but also the proliferation and differentiation of cells inside the construct. If applied to artificial SDV, this approach has a very high potential to simulate the physical and physiological characteristics that SDV should have.

In this study, we combined a dragging 3D printing technique using synthetic polymers with 3D bioprinting using natural polymers containing cells to fabricate an engineered spontaneous cellular assembly small diameter vessel (S-SDV) with a cell layer composition similar to that of an autologous blood vessel (Fig. 1a). The normal 3D printing method provides an easier way to fabricate 3D free form tubular constructs than the conventional methods. However, it is difficult to have sufficient mechanical properties for transplantation while having a uniform endothelial layer on the inner layer [11]. Here, intensifying the dragging 3D printing technique allowed for precise control of the pore size by adjusting the number of columns and feed rate. The pore in the 3D tissue-engineered scaffold has an important role in nutrient transport and metabolism and cell viability. However, with normal 3D printing, it is not possible to create a porous tubular structure without supporting material and post-processing. So, we tried to advance our previously established dragging printing method for controlling pore sizes on the tubular construct. By improving its versatility, we applied this technique to fabricate small diameter blood vessels for regenerative medicine purpose and evaluated its mechanical and biological properties

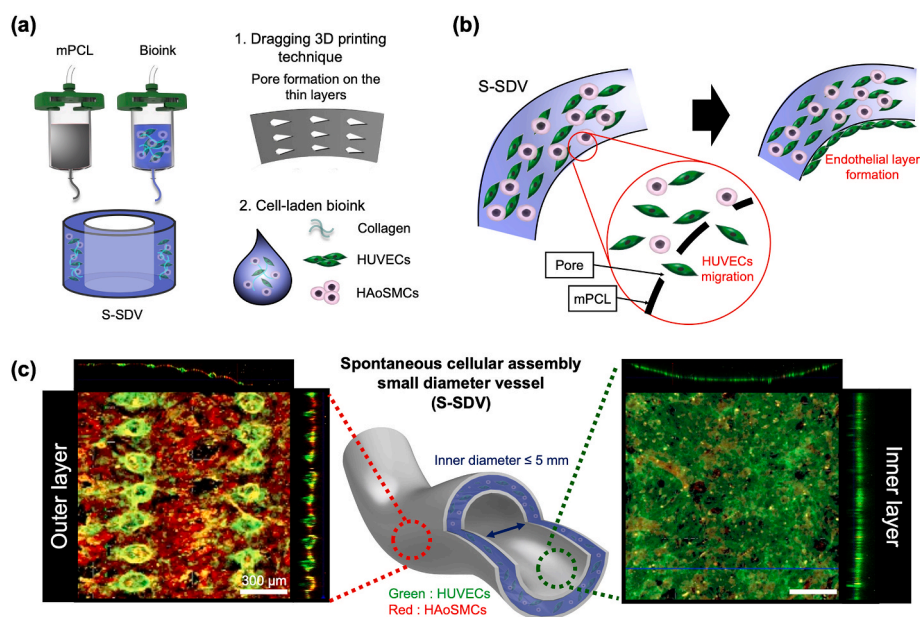


**Fig. 1.** Images of the spontaneous cellular assembly small diameter vessel (S-SDV) fabrication process. (a) Schematics of the fabrication and (b) human umbilical vein endothelial cells (HUVECs) behavior on the S-SDV. (c) The developed artificial small diameter blood vessel graft, S-SDV. Green; HUVECs, Red; human aortic smooth muscle cells (HAoSMCs).

properly. In this study, the pores allowed cells to survive inside the 3D tubular constructs, and affected cell migration and spontaneous assembly, enabling human umbilical vein endothelial cells (HUVECs) to spontaneously form an endothelium on the inner layer of the 3D tubular constructs (HUVEC covered area  $\geq 97.68\%$ ) (Figs. 1b and c). Through this, the adhesion of the platelet could be prevented. In addition, the graft need be flexible, maintained at an appropriate bursting pressure, and be able to withstand the force caused by suturing during surgery. The S-SDVs used in this study had sufficient mechanical properties to the level of native blood vessels, which is ultimate strength of 6–9 MPa, burst pressure of  $432.23 \pm 45.54$  mmHg and suture retention of withstanding a maximum of  $6.69 \pm 1.8$  N tension force.

Generally, to maintain the shape of the construct, other materials are mixed to make a hybrid ink, crosslinking is added by UV irradiation, and a hardening bath is added to the fabrication process. But these methods still have the disadvantage that they contain a sacrificial layer that must be removed for the final tubular construct [30]. However, the dragging 3D printing technique used here enables the fabrication of a construct that satisfies the multi-layered, free-form graft condition [31]. This technique can build the desired physiological construct by sequentially arranging cell-laden bioink printing. The ability and mechanical properties of the graft to mimic the autologous construct also affect the ability of the graft to withstand the physiological environment after transplantation [18]. Therefore, the S-SDV could be an attractive alternative for the fabrication of artificial SDVs.

## 2. Materials and method

### 2.1. Development of a porous free-form multi-layered construct using a dragging 3D printing technique

Dragging 3D printing was performed using a lab-made multi-head bioprinting system. A customized dragging G-code generator program was used to fabricate the various shapes of the porous multi-layered tubular constructs. A medical-grade polycaprolactone (mPCL, Resomer C209, Evonik, Germany) with a molecular weight of 73,000 and an inherent viscosity of 0.8–1.0 dl/g (0.1% in chloroform, 25 °C) was used as the printing material. First, mPCL pellets were placed in a stainless-steel print head (SS10, U-Jin Tech., Republic of Korea) and melted at 85 °C, after which the print bed was heated to 35 °C during printing. In addition, the room temperature (RT) during the printing was maintained at approximately 15–18 °C. After the pellets had completely melted, they were printed on the print bed and dragging region using precision nozzles (SHN-0.1 N, Musashi, Japan) with a size of 150  $\mu\text{m}$  at an equal pneumatic pressure of  $550 \pm 10$  kPa. To obtain a stretching material, the printing feed rate was adjusted such that the printing region was printed at a rate of 8 mm/s, whereas the dragging region was printed at a rate of 150 mm/s. The vertical standoff distance was 100  $\mu\text{m}$ . We investigated the morphological features of the dragging printed 3D construct and compared it with normal 3D printing by field emission scanning electron microscopy (FE-SEM; S-4800, Hitachi, Japan).

To validate the fabrication ability of the multi-layer tubular construct with natural polymer, a 2% porcine skin atelocollagen collagen (Collagen; Dalim Tissen, Seoul, Republic of Korea) was loaded in the space between the porous layers using a 26G nozzle (PN-26G-13, U-Jin Tech, Republic of Korea) with an operating pneumatic pressure of 15 kPa. The collagen was mixed with color inks to clearly distinguish each layer.

### 2.2. Parameter study of the dragging 3D printing technique for pore control

In the dragging technique, one variable of the dragging arc length is directly related to pore control (Supplementary Figs. 1a and b). This variable is determined by adjusting the number of symmetrically arranged columns (Supplementary Figs. 1c–e). Therefore, the dragging arc

length was controlled by adjusting the number of columns (NC), and the pore size change was observed accordingly. Specimens were manufactured with R1 (Inner diameter) = 5.0 mm, R2 (Outer diameter) = 5.2 mm, and the angle of  $\theta 2$  was fixed at 3°. Dragging G-code was produced by adjusting the NC44 to NC28 (Supplementary Fig. 1f).

### 2.3. Analysis of mechanical properties of porous tubular multi-layered constructs

To evaluate the mechanical properties of the constructs with different pore sizes and layer numbers, the specimens were subjected to tensile testing using a universal testing machine (UTM; Model E42, MTS, Germany). The load cell capacity of the UTM was 5.0 KN, and the fixed specimens were elongated at a speed of 0.1 mm/s.

We prepared porous multi-layered tubular constructs with two to five layers to investigate the tensile strength with different layer numbers. The 10 mm length specimens were prepared for the tensile test, with 3.25 mm of each end of the specimens mounted to the UTM jig, and the remaining 3.5 mm were used for the tensile testing. The cross-sectional area of the two to five layers was measured as 2.16 mm<sup>2</sup>, 3.75 mm<sup>2</sup>, 5.67 mm<sup>2</sup>, and 7.89 mm<sup>2</sup>, respectively.

Likewise, to investigate the mechanical properties of the specimens depending on different pore sizes, specimens were prepared for three different NC conditions (NC42 to NC30). The sample jigging was mounted and measured as mentioned above. The cross-sectional area of the specimens was used at 6.40 mm<sup>2</sup> by measuring from FE-SEM analysis to calculate the stress-strain.

### 2.4. Preparation of the spontaneous cellular assembly small diameter vessel

For the fabrication of the S-SDV, an SDV construct was printed with mPCL using a precision nozzle with an inner diameter of 150  $\mu\text{m}$  and 550 kPa pneumatic pressure. The construct has an inner, and outer diameter, and height of 5, 7, and 5 mm, respectively.

A bioink was prepared by mixing the cell pellets with the collagen, and the final concentration of the bioink was 2%. The collagen was neutralized with NaOH and 10X Dulbecco's modified eagle medium (Hyclone, Logan, USA). Primary HUVECs (PromoCell, Heidelberg, Germany) were cultured in an endothelial cell growth medium solution containing endothelial cell growth medium 2 (PromoCell), growth medium supplementmix 2 (PromoCell), and 1% penicillin-streptomycin (P/S; Gibco). Also, primary human aortic smooth muscle cells (HAoSMCs; PromoCell) were cultured in a smooth muscle cell growth medium solution containing smooth muscle cell growth medium 2 (PromoCell), growth medium 2 supplementmix (PromoCell), and 1% P/S. These cells were maintained at 37 °C and 5% CO<sub>2</sub>. The HUVECs and HAoSMCs were detached using trypsin-ethylenediaminetetraacetic acid (Trypsin-EDTA) and centrifuged to obtain cell pellets.

The seeding density of the cells used in the bioink was HUVECs = 10<sup>7</sup>/ml (HUVECs-only); HUVECs: HAoSMCs = 5 × 10<sup>6</sup>: 5 × 10<sup>6</sup>/ml (V1: S1); HUVECs: HAoSMCs = 2 × 10<sup>7</sup>: 5 × 10<sup>6</sup>/ml (V4: S1). For HUVECs-only culturing, the endothelial cell growth medium solution was used. For V1: S1 and V4: S1 culturing, the endothelial cell growth medium solution and the smooth muscle cell growth medium solution were mixed with a 4:1 ratio. All bioinks were prepared under ice-cold conditions. Then, S-SDV was induced by sequentially bioprinting 2% bioink between the inner and outer layers of the SDV construct. The 3D bioprinting used a 26G nozzle at 15 kPa, 4 °C.

### 2.5. Study of the cell behavior according to pore size

To confirm the migration of the HUVECs according to pore size, three NCs of SDV constructs were printed. NC40, NC36, and NC32 had dragging arc lengths of 0.27, 0.31, and 0.37 mm, respectively. The pores were observed using FE-SEM and the results were measured by ImageJ.

After that, the HUVECs-only bioink was injected into the NC40, NC36, and NC32 through 3D bioprinting for inducing S-SDV. These were cross-linked for at least 30 min at 37 °C and 5% CO<sub>2</sub>. The media was added, and these were cultured under the same condition for 1 and 14 days.

HUVECs were stained using Phalloidin-Tetramethylrhodamine B isothiocyanate (Phalloidin; Sigma Aldrich). The specimens were placed in a 4% paraformaldehyde solution for 15 min at RT, after which they were treated with 0.1% Triton X-100 for 15 min. Subsequently, specimens were stained using FITC-phalloidin for 20 min at RT. VECTA-SHIELD® (DAPI; Vector Laboratories, Burlingame, USA) was added for staining the nuclei. The specimens were observed using confocal microscopy (LMS 980, Zeiss, Oberkochen, Germany) and FE-SEM.

## 2.6. Mechanical validation of a small diameter vessel construct

To confirm the leakage of the S-SDV with V4:A1 bioink, 2 μm Fluorescein isothiocyanate-dextran (FITC-microspheres; Sigma Aldrich, St. Louis, USA) were perfused with a 10 mm/s flow rate, similar to bloodstream speed [32]. The S-SDV was connected to the peristaltic pump via a silicone hose. The results were observed in real-time with 365 nm wavelength UV light and intensity analysis was performed with ImageJ.

A burst pressure test was conducted by connecting a silicone hose, which is mounted with a syringe pump, on each end of the S-SDV with V4:A1 bioink. Phosphate buffered saline 1X (PBS; Gibco, New York, USA) was infused in the S-SDV until it completely ruptured and was not detached from a pressure sensor (MSR, Elveflow, France).

Suturing retention was measured by suture on the 6-point each edge. The SDV construct was fixed with a non-absorbable suture thread (USP size 6–0) and a customized UTM jig and it was fastened with a tensile jig (Supplementary Fig. 2). A 0.1 mm/s rate of elongation was used until the specimen was completely torn. All mechanical validations were conducted at RT.

## 2.7. Study of the cell behavior according to cell density

Two kinds of cell ratios (V1:S1, V4:S1) were prepared to investigate the different behavior of cells according to the seeding cell density of S-SDV. The pore size was controlled under NC36. The samples were cultured under the same conditions for 7 and 14 days.

The cells were stained using Immunofluorescence staining to distinguish between the HUVECs and HAoSMCs. Subsequently, the samples were fixed using a 4% paraformaldehyde solution for 10 min, after which they were permeabilized using 0.1% Triton X-100 for 10 min. Thereafter, the samples were treated using 1% bovine serum albumin (BSA) for 30 min for blocking. Subsequently, the HUVECs were stained using primary antibodies and anti-CD31 (Abcam, Cambridge, USA), and the HAoSMCs were stained using anti-α-SMA (Abcam) at a ratio of 1:100 at 4 °C overnight. Thereafter, Alexa Fluor 488 and Alexa Fluor 594 secondary antibodies (Invitrogen, California, USA) were diluted in 1% BSA and applied to the samples for 2 h at RT. The samples were observed using confocal microscopy. We quantitatively analyzed surface covering density, depending on co-culture concentration and cell culturing period, through ImageJ.

## 2.8. Study of the cell behavior according to oxygen concentration

Two experimental groups were prepared to investigate the effect of oxygen concentration gradient on the cell behavior of S-SDV. The pore size was controlled under NC36 and V4:S1. Group 1 was the S-SDV with an inner, and outer diameter, and height of 5, 7, and 5 mm. Group 2 was Group 1 cut in half vertically. These experimental groups were cultured under the same conditions for 7 days.

To distinguish between the HUVECs and HAoSMCs, the cells were stained the same way as mentioned above. The groups were observed

using confocal microscopy. In addition, the area of the HUVECs on each layer was quantitatively analyzed through ImageJ.

## 2.9. Numerical analysis of oxygen concentration

Oxygen concentration distribution around the S-SDV construct was analyzed by a numerical simulation software, COMSOL Multiphysics 5.3a (COMSOL Inc, Burlington, USA). To compare the oxygen concentration distribution depending on the shape of the S-SDV construct, two different shapes of the S-SDV construct were applied in the analysis: full-tube (Group 1) and half-tube (Group 2) shapes.

To model the diffusion and consumption of oxygen by the S-SDV construct, the Transport of Diluted Species module was used in COMSOL. The initial oxygen concentration of the medium and S-SDV construct and oxygen concentration on the top boundary was set as 0.2 mol/m<sup>3</sup>. Diffusion coefficients of oxygen in the medium and the S-SDV construct were assumed to be 2.0 and 6.0 × 10<sup>-9</sup> m<sup>2</sup>/s, respectively. Based on research performed in similar studies [33], the oxygen consumption model was applied to the S-SDV construct using Michaelis-Menten reaction kinetics. In this model, the mass balance of oxygen can be described by Fick's second law with a reaction term as follows:

$$\frac{\partial C(z, t)}{\partial t} = D \frac{\partial^2 C(z, t)}{\partial z^2} - R(z, t) \quad (1)$$

where C is the oxygen concentration as a function of space and time, and D is the diffusion coefficient of oxygen. R represents the oxygen consumption rate per unit volume and can be described by the following equation:

$$R(z, t) = \frac{OCR_{\max} \times C(z, t)}{C(z, t) + Cmm_{O_2}} \quad (2)$$

where OCR<sub>max</sub> and Cmm<sub>O<sub>2</sub></sub> represent the maximum oxygen consumption rate and the Michaelis-Menten reaction constant for the oxygen consumption by the cells in the S-SDV construct, respectively. Based on a previous study [34], the Cmm<sub>O<sub>2</sub></sub> and OCR<sub>max</sub> were assumed to have 0.005 mol/m<sup>3</sup> and (6.367 × 10<sup>-17</sup> mol/s) × (cell density), respectively, while cell density was set as 5 million/cm<sup>3</sup>. The time-dependent oxygen distribution was analyzed between 0 and 10,000 s with a step of 2500 s.

## 2.10. Analysis of antiplatelet adhesive behavior

An experiment was prepared to check whether the antiplatelet adhesive behavior occurs when platelets in the blood pass through the S-SDV. The used blood from 3 donors is single-donor human whole blood that was purchased from Innovative Research, Inc. (Novi, MI, USA). The blood was treated with sodium citrate 3.8%, an anticoagulant.

S-SDV and cell-free SDV were prepared for comparison and NC36 was used. In the S-SDV, the cell density was V4:S1. The cell-free SDV construct was only 2% collagen without HUVECs and HAoSMCs inside. These were connected to a perfusable pump with a silicon hose, respectively. The prepared samples were perfused with blood for 10 min [22], then, non-adhered platelets were washed away with PBS for 3 min.

Platelets attached to the samples were confirmed by immunofluorescence staining with CD41a (Abcam) antibody. To distinguish the HUVECs, the red fluorescent protein-expressing human umbilical vein endothelial cells were used (RFP-HUVECs; Anglo-Proteomie, Boston, USA). The HAoSMCs were not stained. The samples were fixed using a 4% paraformaldehyde solution for 10 min, after which they were permeabilized using 0.1% Triton X-100 for 10 min. Thereafter, the samples were treated using 1% BSA for 30 min for blocking. Subsequently, the platelets were stained using primary antibodies and anti-CD41a at a ratio of 1:100 at 4 °C overnight. Thereafter, Alexa Fluor 488 secondary antibody was diluted in 1% BSA and applied to the samples for 2 h at RT. The samples were observed using confocal microscopy.

## 2.11. Statistical analysis

The obtained images were analyzed using ImageJ (National Institutes of Health, Bethesda, USA). Data processing and statistical analysis were performed using GraphPad Prism 9 (GraphPad Inc, San Diego, USA). The statistical analysis data were expressed as the mean  $\pm$  standard deviation. For the comparison between the two experimental groups, a student's t-test and one-way analysis of variance (ANOVA) was performed.

## 3. Results

### 3.1. Fabrication of the porous, free-form, multi-layered construct using the dragging 3D printing technique

In a normal 3D printing method, the diameter of the extruded strand depends on the nozzle's inner diameter (Fig. 2a). As shown in the results, the 150  $\mu$ m thick wall fabricated by the normal 3D printing is comprised of stacked mPCL strands without pores (Figs. 2b and c). It was also confirmed that the printed mPCL strands had uniform thicknesses (Fig. 2d). On the other hand, the wall fabricated by the dragging 3D printing technique enables the formation of pores; the top view image also confirmed that dragged mPCL strands allowed strand stretching and connection to each other's column (Figs. 2e–h). Thus, there are distinct morphological differences that induced pores between the normal and the dragging 3D printing techniques (Fig. 2i).

### 3.2. Fabrication of the free-form porous construct using the dragging 3D printing technique

Using the customized dragging G-code program, porous free-form constructs were fabricated with mPCL. A porous tubular construct with a bellow pattern was fabricated (Left) similar to a commercial artificial SDV (Right) used clinically (Fig. 3a). In addition, it was confirmed that small diameter tubular constructs with the bellow

pattern could be manufactured with inner diameters of 5 and 2 mm, respectively (Figs. 3b and c). The bellow patterned tubular constructs created by the dragging 3D printing technique were porous and thin (Thickness  $\leq$ 100  $\mu$ m), enabling flexibility and recovery from bending motions (Fig. 3d). In addition, by adjusting the dragging pattern, tubular constructs with helical, zigzag, and star shapes, as well as Y-shaped small diameter and multi-layer constructs, can be fabricated (Figs. 3e–i).

Tubular constructs with high aspect ratios (Inner diameter of 5 mm, height of 80 mm) could also be produced (Fig. 3j). In this study, porous membranes with 2 and 3D shapes (Thickness  $\simeq$  of 80  $\mu$ m) were also fabricated using the dragging 3D printing technique (Fig. 3k).

### 3.3. Fabrication of the multi-layered tubular porous construct using the dragging 3D printing technique

The multi-layered tubular constructs were fabricated with 2–5 layers via the dragging 3D printing technique (Fig. 4a). In addition, the placement of the 2% collagen mixed with the color inks between each layer was visually confirmed (Fig. 4b). The tensile test showed that the load value tended to increase as the number of layers increased, and 2 to 5 layers withstood 16.1, 26.6, 46.6, and 59.7 N depending on the number of layers, respectively (Fig. 4c). Based on the stress-strain curve, Young's modulus was measured at around 200 MPa but there was no significant difference between each number of layers. The ultimate strength was present at 6–9 MPa depending on the number of layers (Fig. 4d).

### 3.4. Control of the pore size on the tubular porous construct using the dragging 3D printing technique

To verify that the pore size could be controlled by adjusting the dragging arc length, the morphology of the pore was investigated using FE-SEM analysis. The results revealed that no pore was formed in using NC44 which had a dragging arc length of 0.23 mm. However, the pores were shown from the NC42 that had a dragging arc length of 0.25 mm

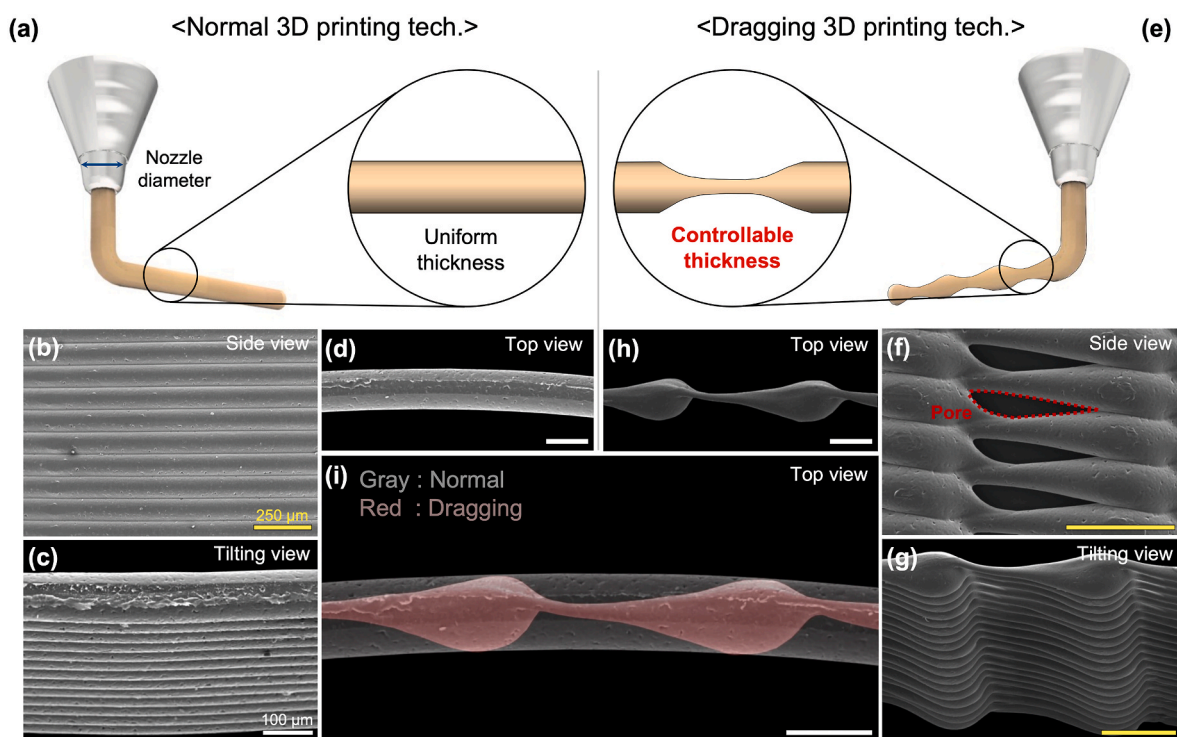


**Fig. 2.** Comparison of the normal and dragging 3D printing technique. Schematics and field emission scanning electron microscopy (FE-SEM) images of the (a–d) normal and (e–h) dragging 3D printing technique. (i) An overlapping FE-SEM image about a strand of the normal and dragging 3D printing technique.

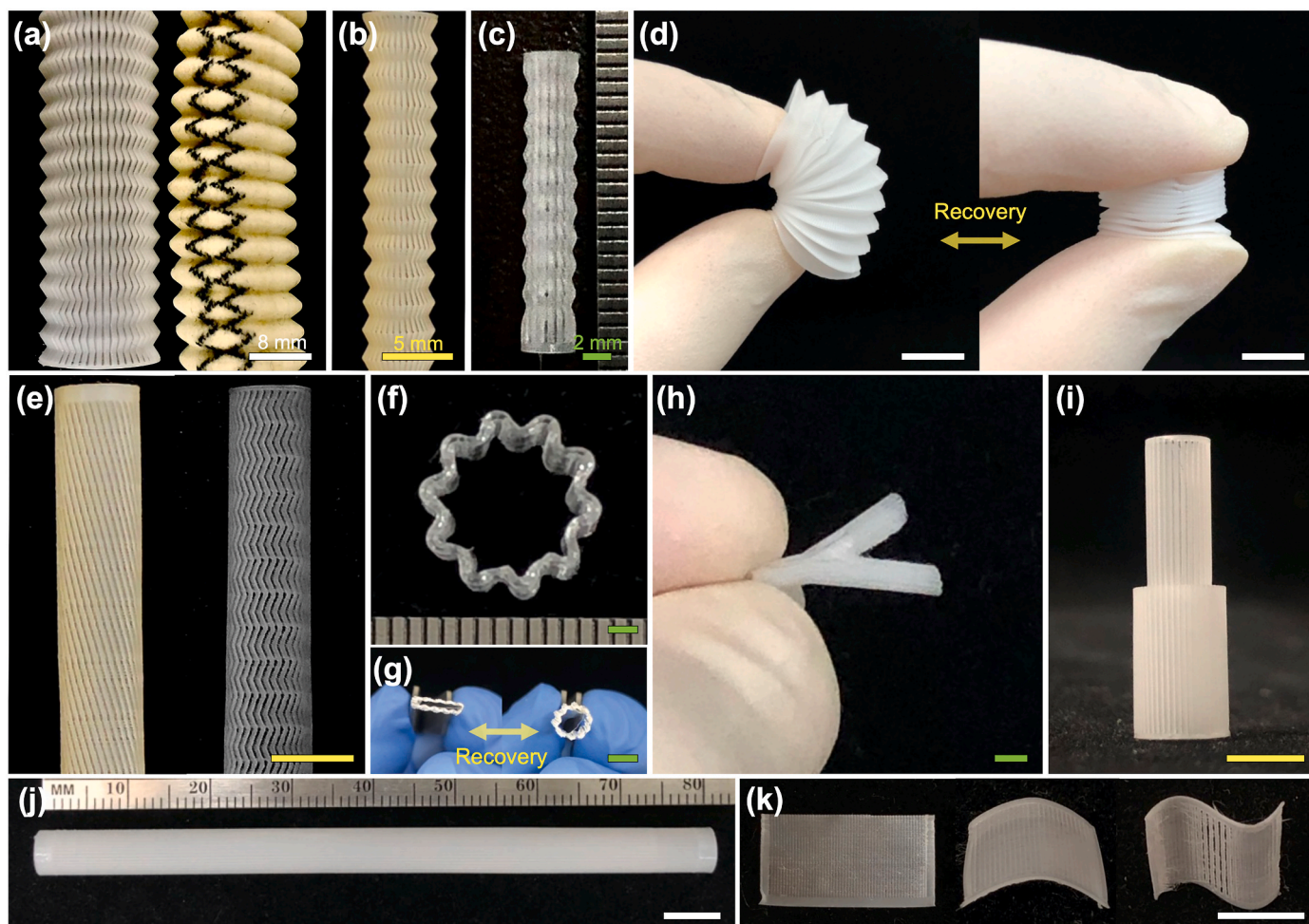


**Fig. 3.** Free-form porous tubular 3D constructs by the dragging 3D printing technique. (a) A commercial artificial SDV (Right) and the mimic's construct (Left). Bellow shape constructs with an inner diameter of (b) 5 mm, (c) 2 mm and (d) capability of reversible bending motions. (e) Complex pattern constructs with helix (Left), zigzag (Right). (f) Wrinkle shape and (g) its reversible stretching motions. Complex shape constructs with (h) a branch and (i) multi-layers, and (j) a high-aspect ratio construct (Inner diameter = 5 mm/height = 80 mm). (k) 2D-3D thin membrane porous constructs (Thickness  $\approx$  80  $\mu$ m).

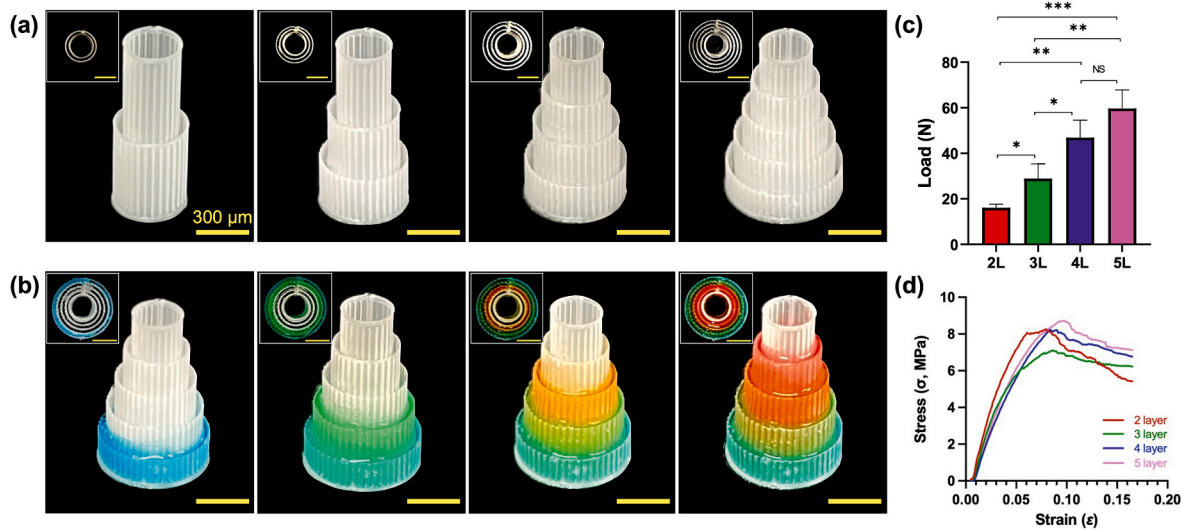


**Fig. 4.** Images of the (a) multi-layered tubular porous constructs using the dragging 3D printing technique, and (b) loaded natural polymers on each layer. (c) A load response and (d) a stress-strain curve according to the layer numbers of the multi-layered porous tubular constructs. L; layers, \* $p < 0.05$ , \*\* $p < 0.01$ , \*\*\* $p < 0.001$ ,  $n \geq 3$ .

and the pore size gradually increased as the NC was decreased to NC30 (Fig. 5a).

For quantitative comparison, the area ( $A$ ), height ( $h$ ), and length ( $l$ ) of the pores were measured and compared (Fig. 5b). The area of the pores using NC42 to NC30 was  $835.0 \pm 79.4$ ,  $2586.0 \pm 156.0$ ,  $3810.0 \pm 485.0$ ,  $6105.4 \pm 169.2$ ,  $8518.0 \pm 311.0$ ,  $11,142.0 \pm 378.0$ , and  $14,142.1 \pm 920.3 \mu\text{m}^2$ , respectively (Fig. 5c). The height of the pores showed that NC42 to NC30 was  $15.4 \pm 0.7$ ,  $26.4 \pm 1.4$ ,  $33.0 \pm 2.0$ ,  $40.1 \pm 1.0$ ,  $49.5 \pm 1.4$ ,  $56.0 \pm 5.0$ , and  $59.4 \pm 3.8 \mu\text{m}$ , respectively (Fig. 5d). Additionally, the length of the pore revealed NC42 to NC30 was  $37.4 \pm 4.2$ ,  $155.2 \pm 4.5$ ,  $176.0 \pm 1.0$ ,  $227.5 \pm 2.3$ ,  $264.4 \pm 2.6$ ,  $294.0 \pm 6.0$ , and  $344.4 \pm 6.8 \mu\text{m}$ , respectively (Fig. 5e).

To evaluate the mechanical strength of the tubular constructs using different NCs, the specimens without cells were subjected to a tensile test. According to the stress-strain curves, the ultimate strengths of NC42, NC36, and NC30 constructs were 0.84, 0.84, and 0.79 MPa, respectively (Fig. 5f).

### 3.5. Fabrication of the spontaneous cellular assembly small diameter vessel via pore and endothelial cells' behavior

The purpose of this study was to determine how the pores formed by dragging 3D printing technique affect HUVECs behavior. To test this, SDV constructs with NC40, NC36, and NC32 were prepared. The pore size was observed by FE-SEM. Pores were measured for the length, height, and area in the inner and outer layers (Supplementary Fig. 4a). The size differences between NC40 and NC36 were 1.6–1.9 times in length and 1.6–2.1 times in height. The area was  $2000 \mu\text{m}^2$  for NC40 and  $6000 \mu\text{m}^2$  for NC36, and the area of NC36 was three times larger than NC40. The NC36 was 0.5–0.6 times in length and 0.9–1.0 times in height smaller than NC32. The area of NC36 was 1.65 times smaller than NC32 (Supplementary Fig. 4b).

The HUVECs-only bioink was injected into the SDV construct by 3D bioprinting. After 1 and 14 days of culture, the pores and the surroundings of the inner layer at the lumen surface side were observed using a confocal microscope (Fig. 6a). HUVECs could be identified on the inner layer even on day 1. After 14 days, it could be observed clearly.

Endothelium was most formed in NC36, followed by NC32 and NC40. Actually, the spontaneous cellular assembly of HUVECs shows different results for each pore size. By analysis of the confocal images on day 14, it was confirmed that the HUVECs covering the surface were formed by approximately  $33.850 \pm 6.67\%$  in NC40,  $81.62 \pm 4.41\%$  in NC36, and  $54.55 \pm 8.36\%$  in NC32 (Fig. 6b). In NC40, it could be

observed that the HUVECs migrated through the pores and grew on the surface but were not yet covered the surface of inner layer. In NC32, it could be observed that the HUVECs migrated but not yet covered the pore of the inner layer. However, in NC36, not only the filled surface but also the pores were covered by the HUVECs (Fig. 6c).

### 3.6. Mechanical validation of the spontaneous cellular assembly small diameter vessel

We next wanted to determine whether the S-SDV construct created by the dragging technique had enough mechanical rigidity to be an implantable small diameter blood vessel graft. Therefore, mechanical testing including leakage, burst pressure, and suture retention was performed. The leakage test found that the FITC-microspheres flowed well into the SDV construct without any rupture or leakage (Fig. 7a, Supplementary Video 1). For the quantitative validation, we compare the fluorescence intensity between the PBS bath and S-SDV. The result of fluorescence intensity was  $6.88 \pm 0.7$  in the PBS bath and  $184.66 \pm 7.2$  in the S-SDV (Fig. 7b). This result suggests that S-SDV has sustainable flow ability without any leakage. Burst pressure analysis revealed that the SDV construct containing 2% collagen bioink withstood over 400 mmHg, whereas without bioink did not withstand the internal pressure at all (Fig. 7c). The suture retention result showed that the SDV construct could withstand a maximum of 8.77 N tension force (Fig. 7d).

Supplementary video related to this article can be found at <https://doi.org/10.1016/j.bioactmat.2023.07.021>

### 3.7. Effect of the cell density for inducing the spontaneous cellular assembly small diameter vessel

To mimic a native blood vessel architecture [35], collagen ink with HUVECs and HAoSMCs, cells that comprise blood vessels, was injected in NC36. To efficiently observe the behavior of the co-cultured cells and increase the rate of layer formation, the experiment was performed by controlling the number of cells. HUVECs and HAoSMCs were mixed in collagen at V1:S1 and V4:S1. The cells were co-cultured and observed by a confocal microscope on days 7 and 14. Immunofluorescence staining was used to distinguish between HUVECs and HAoSMCs as green and red, respectively. When the cell density ratio of HUVECs and HAoSMCs was V1:S1, it was confirmed that HAoSMCs actively migrated regardless of the inner and outer layers over time (Fig. 8a). HUVECs were barely observable in the inner and outer layers. Quantitative results are presented showing that HUVECs covered inner surface  $16.7 \pm 1.2\%$  and

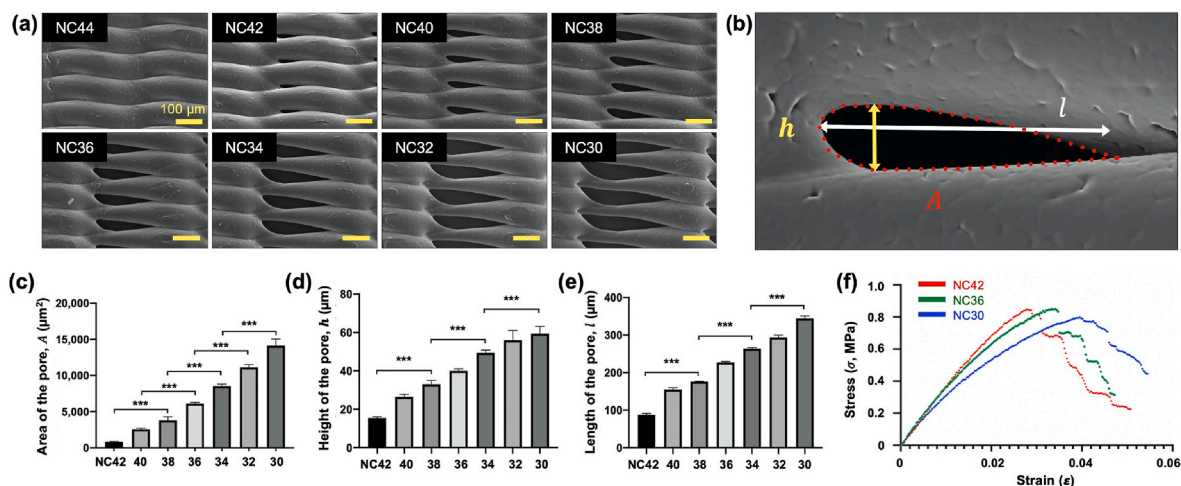
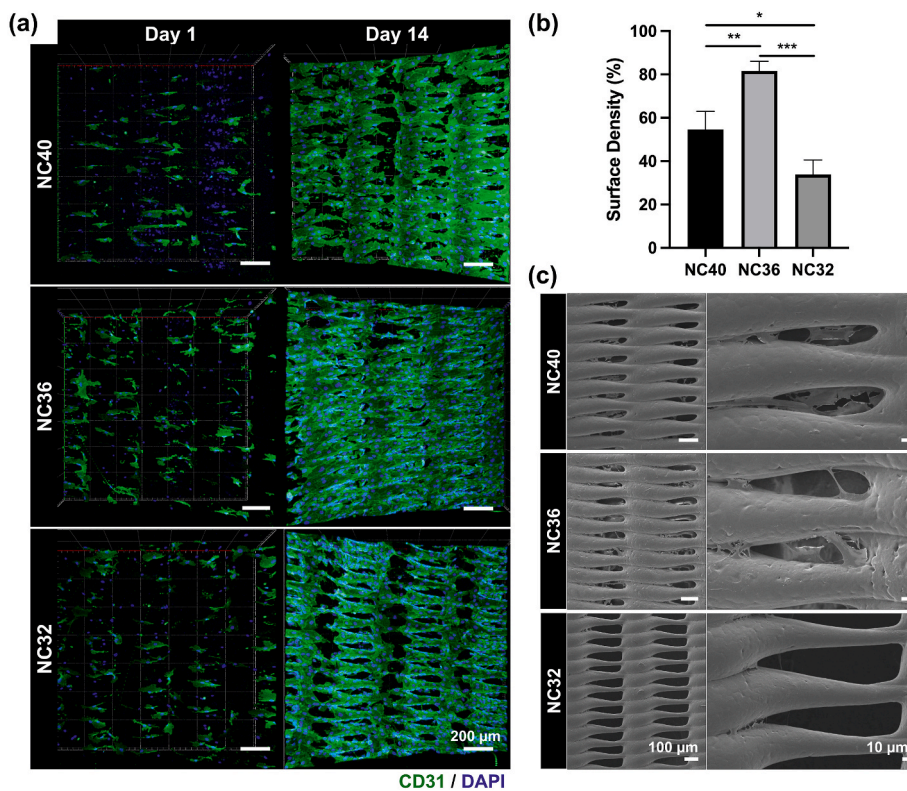


Fig. 5. (a) Field emission scanning electron microscopy (FE-SEM) images of the pore morphology by the number of columns (NC). (b–e) Quantitative comparison of the area ( $A$ ), height ( $h$ ), and length ( $l$ ). (f) A stress-strain curve according to the NC. Red; NC42, Green; NC36, Blue; NC30,  $***p < 0.001$ ,  $n \geq 3$ .



**Fig. 6.** (a) Confocal images of the inner layer on NC40, NC36 and NC32 with HUVECs-only bioink culturing for 1 day and 14 days. Green; CD31, Blue; DAPI. (b) An analysis graph about the HUVECs surface density and (c) field emission scanning electron microscopy images of the (a) at day 14. \* $p < 0.05$ , \*\* $p < 0.01$ , \*\*\* $p < 0.001$ ,  $n = 3$ .

19.6 ± 1.87% for 7 days, 14 days, representatively. Also, outer surface covered 1.07 ± 0.38% and 9.12 ± 0.74% for 7 days, 7 days representatively (Fig. 8d).

In the case of V4:S1, different results were shown depending on each layer (Fig. 8b). The result of HUVEC' active movement was mostly observed on the inner layer. Notably, after 14 days, HUVECs spontaneously migrated through the pores to the inner layer, forming a

spontaneously assembled dense layer. HAoSMCs were observed in both inner and outer layers but were predominantly present in the outer layer (Fig. 8c). Quantitatively, inner surface was covered 75.95 ± 1.2%, contritely outer was surfaced 1.01 ± 0.3% for 7 days. For 14 days, almost inner surface was covered as 97.68 ± 0.4% through HUVEC's migration and outer surface covered 26.68 ± 5.6% (Fig. 8d).

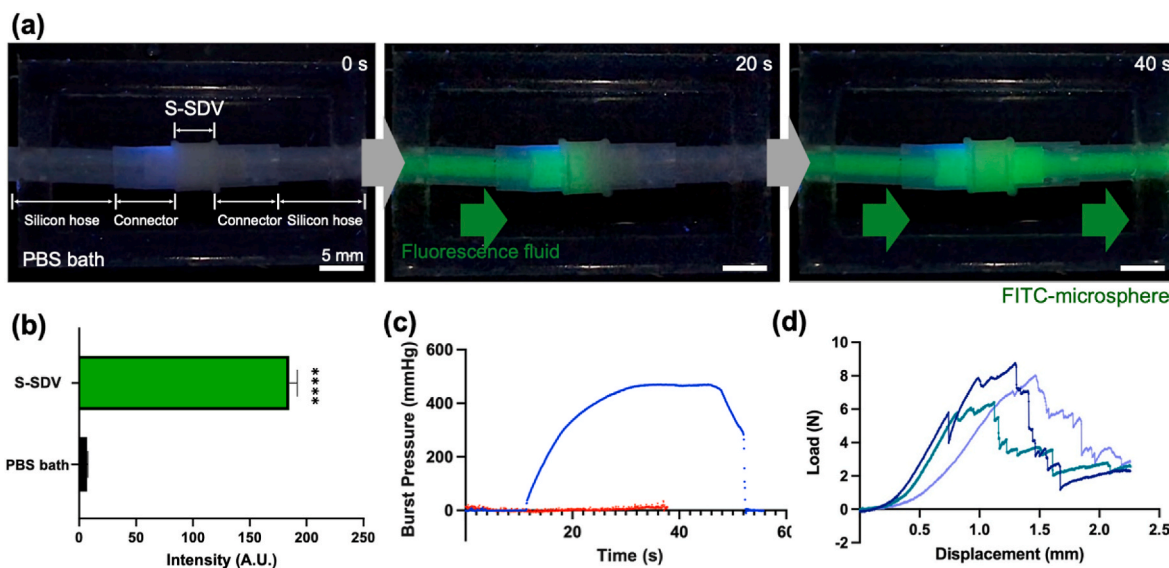


**Fig. 7.** Mechanical validation results; (a) Real-time images and (b) the fluorescent intensity analysis of leakage test by the fluorescent flow in the S-SDV. Green; FITC-microsphere. \*\*\* $p < 0.0001$ . (c) Burst pressure graph of the S-SDV. Orange: SDV construct (w/o cell-laden bioink), Blue: S-SDV (w/cell-laden bioink) (d) A suture tension analysis of the SDV construct.  $n = 3$ .

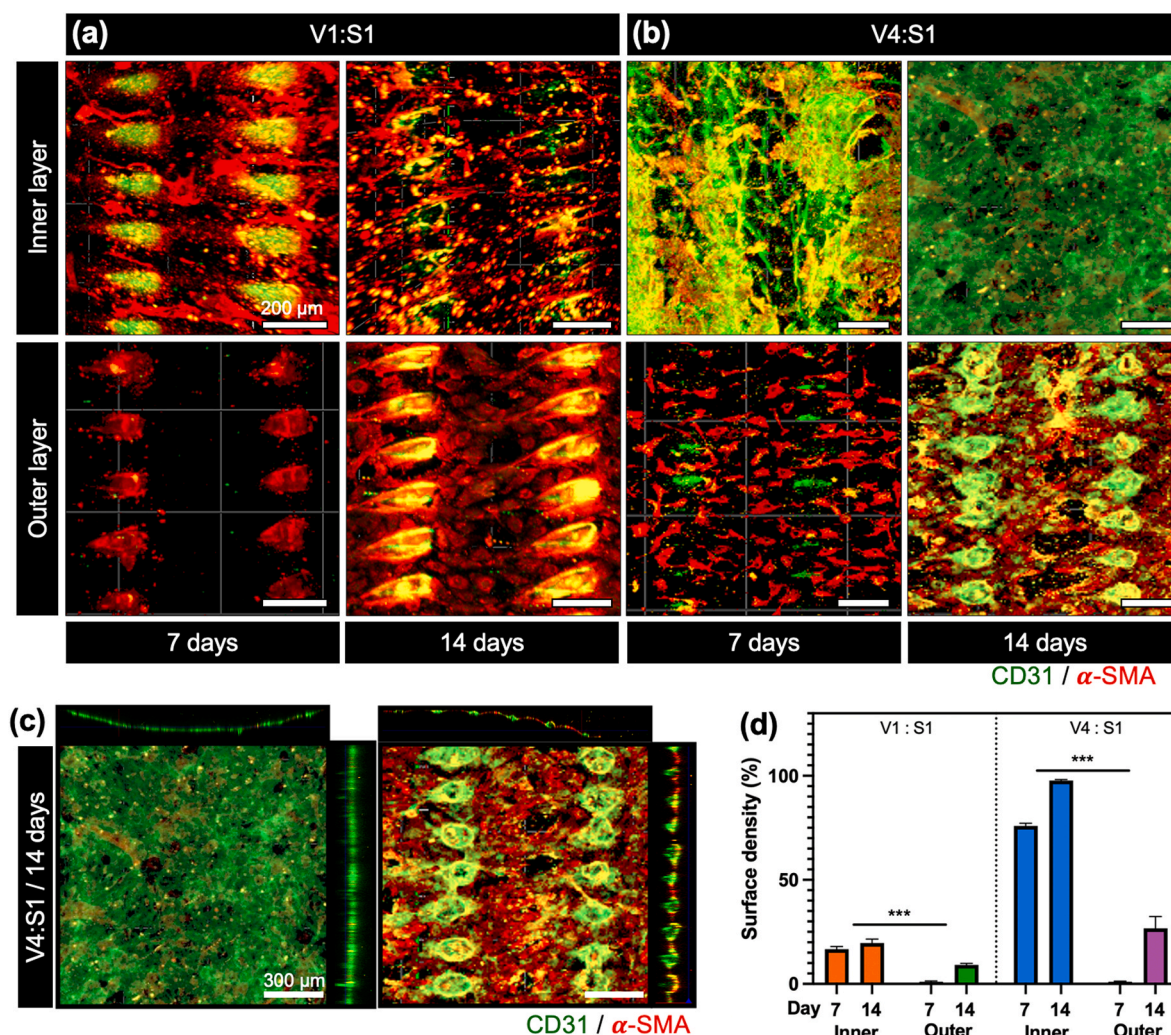


**Fig. 8.** Confocal images of spontaneous cellular assembly small diameter vessel (S-SDV) with human umbilical vein endothelial cells (HUVECs) and human aortic smooth muscle cell (HAoSMCs) encapsulated bioink culturing on 7, 14 days. The HUVECs:HAoSMCs density ratio is (a) V1:S1 and (b) V4:S1. (c) Magnified confocal images of the V4:S1 on 14 days. The left image shows the inner layer, and the right image shows the outer layer of the S-SDV. Green; HUVECs, Red; HAoSMCs. (d) Quantitative analysis of the surface density through HUVEC's cells,  $***p < 0.001$ ,  $n \geq 3$ .

### 3.8. Effect of oxygen concentration for inducing the spontaneous cellular assembly small diameter vessel

In NC36 and V4:S1 conditions, HUVECs mainly migrated to the inner layer. To investigate the cause, Group 1 and Group 2 and treated with different oxygen concentration gradients and the movement of HUVECs and HAoSMCs was observed. HUVECs were stained in green and HAoSMCs were stained in red by immunofluorescence staining. The difference in oxygen concentration gradients of Group 1 and Group 2 was confirmed through simulation (Figs. 9a, b and Supplementary Videos 2, 3). In Group 1, oxygen was rapidly depleted in the tube-shaped inner layer, but in Group 2, the open inner layer had almost the same oxygen concentration as the outer layer. Based on this, an actual experiment was conducted (Fig. 9c). We observed that HAoSMCs from Groups 1 and 2 migrated into the inner and outer layers regardless of the oxygen concentration gradient. In contrast, HUVECs were observed more frequently in the inner layer of Group 1, which had the relatively lowest oxygen concentration gradient. By analyzing the confocal results, the area where the migrated HUVECs were distributed in each layer was calculated (Fig. 9d). The inner layer of Group 1 was 2.15 and the outer was 0.11. Group 2 was 0.66 in the inner and 0.74 in the outer layer. It was confirmed that Group 1 was 2.15, which was 3.26 times higher than Group's 0.66. Even within Group 1, the rate of movement to the inner

layer was 19.55 times higher than that of the outer layer. Within Group 2, the rates of the area of the outer and inner layers were almost similar at 0.89.

Supplementary video related to this article can be found at <https://doi.org/10.1016/j.bioactmat.2023.07.021>

### 3.9. Anti-platelet adhesion

A crucial component of an artificial SDV graft is a well-formed endothelium to prevent the adhesion of platelets. To examine platelet adhesion in the S-SDV, whole blood flowed into the S-SDV, and adhesion of the platelets on the inner layer was observed (Fig. 10a). A cell-free SDV, an SDV construct filled only with collagen without cells, was also prepared for comparison. RFP-HUVECs were used, platelets were stained green, and HAoSMCs were not stained.

In the case of the S-SDV, the platelets were barely invisible. In contrast, in the cell-free SDV, it was confirmed that a large number of platelets were observed (Fig. 10b). By quantifying the number of attached platelets, it was confirmed that the platelets count in cell-free SDV was significantly higher (Fig. 10c). The adhered platelets were observed in each condition. However, the morphology of the platelets showed a much tighter attachment and a more activated form in the cell-free SDV compared to the S-SDV (Supplementary Fig. 3) [36].

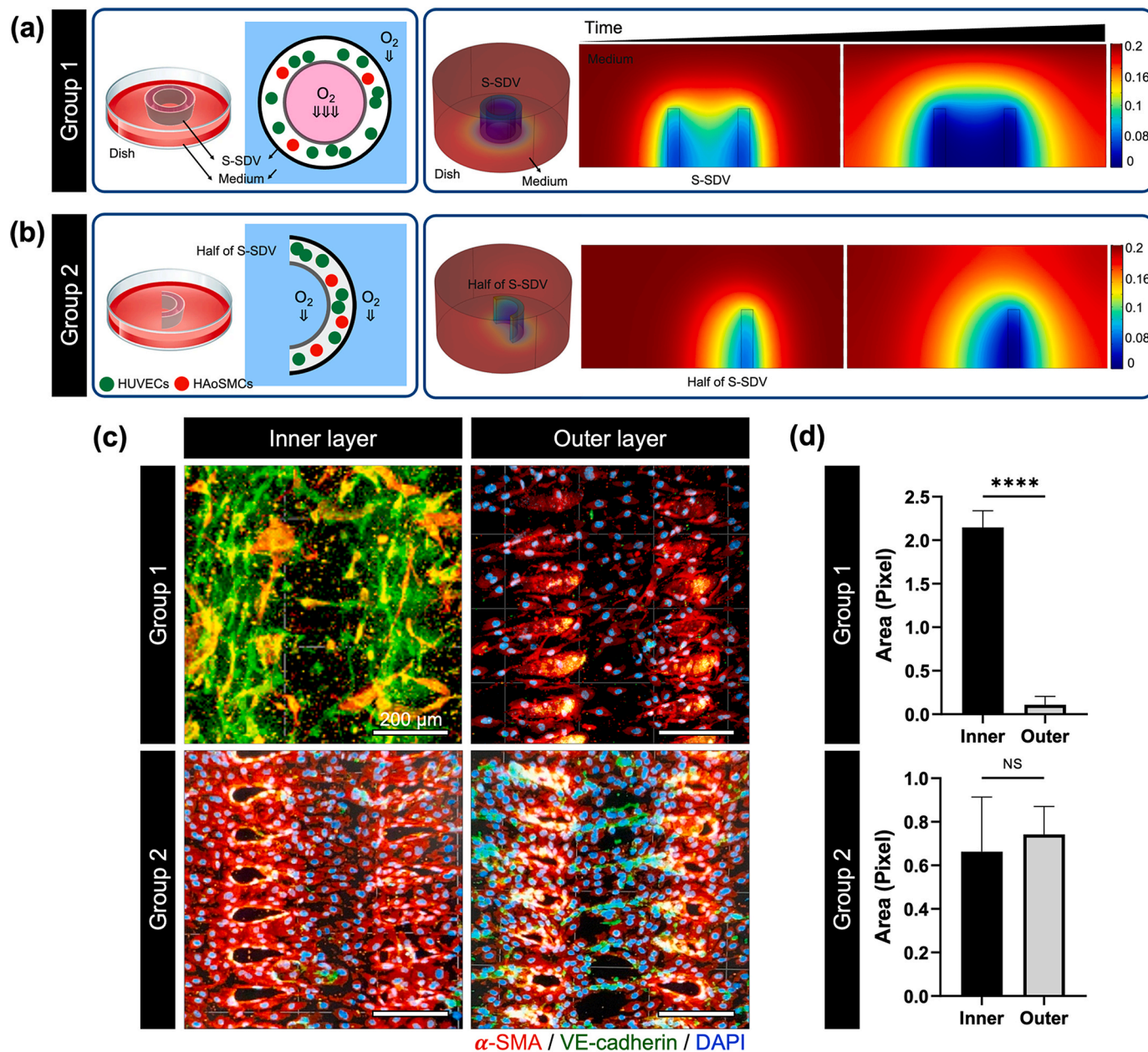


**Fig. 9.** Experimental design and 2D, 3D numerical analysis results of (a) Group 1's and (b) Group 2's oxygen concentration. (c) Confocal images of the experimental results of the Group 1 and Group 2. A spontaneous cellular assembly small diameter vessel (S-SDV) with human umbilical vein endothelial cells (HUVECs) and human aortic smooth muscle cells (HAoSMCs) laden bioink culturing on 7 days. Green; HUVECs, Red; HAoSMCs, Blue; DAPI. (d) The area graphs of HUVECs on the inner and outer layers of Group 1 and Group 2. \*\*\*\* $p < 0.0001$ ,  $n = 3$ .

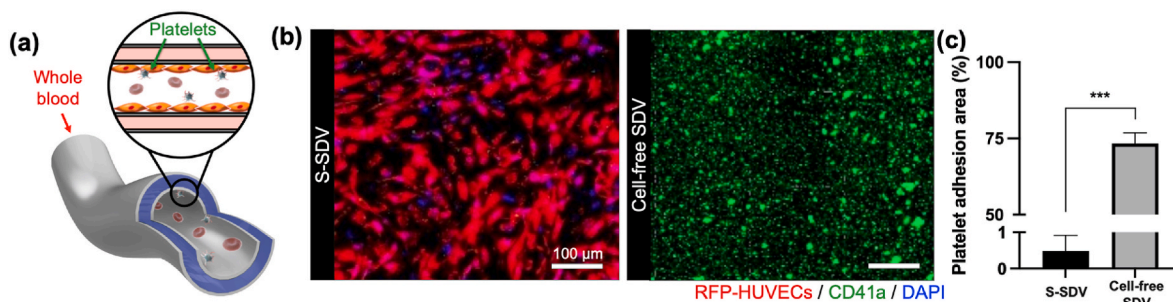


**Fig. 10.** (a) A schematic of the blood flow and platelet adhesion. (b) Confocal images about the anti-platelet adhesion of the spontaneous cellular assembly small diameter vessel (S-SDV) with human umbilical vein endothelial cells (HUVECs), human aortic smooth muscle cell (HAoSMCs) and cell-free SDV. Red; RFP-HUVECs, Green; platelets, Blue; DAPI. (c) Quantitative analysis of the platelet adhesion area. \*\*\* $p < 0.001$ ,  $n = 3$ .

#### 4. Discussion

In 3D constructs for tissue engineering, pores are one of the essential factors to be considered because they play an important role in cell metabolism [2,37–40]. However, other studies were able to manufacture pores only by using additional equipment or sacrificial materials [41]. By developing a dragging 3D printing technology in previous research, it was easy, and effectively possible to fabricate a tubular construct with pores without additional processing [31]. In addition, it was observed that cell growth in the tubular construct with pores was more effective than in the absence of pores [31]. Here, we developed advanced dragging 3D printing technology that could control the pore size of the tubular construct by adjusting the design parameters. The results revealed that pores with a length of approximately 344  $\mu\text{m}$  were produced when a 150  $\mu\text{m}$  nozzle was used with NC30 (Dragging arc length of 400  $\mu\text{m}$ ). In contrast, no pore was formed at NC28 (Dragging arc length of 430  $\mu\text{m}$ ), which could be attributed to the fact that the column was not connected to each other column. The smallest pore with a length of approximately 37.4  $\mu\text{m}$  was formed using NC42 (Dragging arc length of 250  $\mu\text{m}$ ). In addition, constructs made with NC44 (Dragging arc length of 230  $\mu\text{m}$ ) had no pores formed. Consequently, the largest pore was obtained when the dragging length was approximately 2.6 times larger (NC30) than the inner diameter of the nozzle, and the smallest pore was obtained when the dragging length was approximately 1.6 times larger (NC42) than the inner diameter of the nozzle. In this regard, the pore size could be different depending on the printing materials. As the dragging technique uses the material's stretch property, it is judged that the viscosity of the material affects the pore formation. In this study, an artificial SDV was proposed that was fabricated by this advanced dragging 3D printing technique. The most important two things in the artificial SDV are to have mechanical properties that can be implanted clinically and to mimic the structure and characteristics of natural blood vessels' endothelium [42]. Many efforts have been made to meet these challenges, but ours is the first study to successfully create a strong and porous S-SDV that can also easily mimic the endothelium.

First of all, in this technology, the material used as the artificial SDV has sufficient mechanical properties. In other studies, natural polymers were used a lot because endothelium was not easily constructed when artificial SDV was made only with synthetic polymers. However, most of the implants developed with natural polymers had weak mechanical properties compared to native blood vessels [43]. Here, by using a synthetic polymer as a frame, the mechanical properties were able to better model the characteristics of blood vessels. mPCL was used as a synthetic polymer for S-SDV. It is a non-toxic, biocompatible polymer that does not release harmful substances to living cells. It has been approved by the FDA and synthesized in a GMP facility, so it is adaptable for clinical application. Our results in filling the inside of the multi-layer with bioinks using natural polymer suggests the possibility of fabricating multi-functional SDV constructs using additional biomolecules that are beneficial to cells in the future. Our findings ensure reliable mechanical properties, enabling easy application in implantation. Given that the ultimate strength of the internal mammary artery is 4.3 MPa, the S-SDV has sufficient mechanical properties (Ultimate strength 6–9 MPa) to withstand physiological stress [44]. The S-SDV has less burst pressure value than native small diameter blood vessel tissue. However, given normal bloodstream pressure is 80–120 mmHg, the S-SDV withstanding an internal pressure over 400 mmHg suggests that it can be sufficiently implantable level [45]. The leakage and suture retention test results show that even though S-SDV has pores, it can replace the function of transporting blood without any leakage.

Natural blood vessels have an endothelium, which plays an important role in keeping blood streaming, enduring blood pressure, and preventing clots [46]. In general, static seeding of endothelial cells into tubular constructs is a traditional and accessible method for endothelial formation. This method has low seeding efficiency, and it is very difficult to form a uniform layer of cells [47,48]. To this, additional seeding, fabrication, and culture techniques are required, which reduce the

productivity and functionality of the construct. Therefore, the remodeling of the endothelium is currently the biggest bottleneck in manufacturing commercial artificial SDV constructs.

However, in this study, the endothelium was automatically formed in the innermost layer of the S-SDV without an additional induction step. The pores allow the passage of cells out of the construct to form the endothelium. HUVECs migrated from the collagen and exited the pore, attaching to the inner layer and the lumen surface, and spontaneous cellular assembly without external intervention.

It has different outcomes in endothelial formation depending on the pore size. First of all, in the case of NC32, the pores are relatively large, so the cells cannot cover the pores even for 14 days. HUVECs cover the pores and the surface in the case of NC40, but because the pores are relatively small, it limits the range of cell migration and growth, leaving uncovered areas on the surface. In contrast, in the case of NC36, it was observed that most of the surface and pores were covered. Not only found the most suitable pore size but also revealed that controlling the pore size is essential for facilitating spontaneous cellular assembly and promoting efficient and consistent endothelium formation for S-SDV.

Furthermore, this behavior was also controlled by the difference in oxygen concentration inside and outside the S-SDV. In general, HUVECs' behavior is significantly affected by surrounding oxygen concentration [49–51]. When cells grow and consume oxygen in a tubular construct, a decrease in oxygen concentration can occur more quickly in the inner layer, which is in contact with the small amount of culture media in a confined space compared to the outer layer. This naturally induced environment creates different oxygen concentration gradients between the inner and outer layers, which could promote the HUVEC's migration toward the inner layer. The simulation result of the oxygen concentration gradient via two different types of models (Full-tube and half-tube) strongly supports its possibility (Fig. 9 and Supplementary videos 2, 3). Therefore, these results suggest that we have developed a flexible, convenient, and reliable method for the fabrication of endothelium.

The spontaneously assembled endothelium is located in the inner layer of the S-SDV and directly interacts with the blood. The endothelium reduces the risk of graft failure due to occlusion and helps regenerate blood vessels through the production of ECM proteins [45]. The endothelium has the property of preventing platelet adhesion, aggregation, and thrombus formation [52]. When human blood flowed on S-SDV, it was confirmed that platelet adhesion hardly occurred, while the construct without endothelium could not prevent platelet adhesion.

#### 5. Conclusion

The dragging technique enables the multi-layered tubular construct with a controllable pore size without any supporting material or device. By controlling the pore size, we confirmed that HUVECs could be layer formation passing through the pore construct on the artificial S-SDV. The oxygen concentration gradient test confirmed that the migration direction of HUVECs co-cultured with HAoSMCs was due to the low oxygen concentration. It was verified that the HUVECs layer formed by the pores and this autonomous movement prevented platelet adhesion. Also, The S-SDV allows blood flow without any leakage and has sufficient flexibility, burst pressure, and suturing tension for transplantation. Consequently, we can fabricate the S-SDVs to contain HUVECs and HAoSMCs with similar physiological cell layers of native blood vessel tissue.

3D multi-layered tubular structure by making the dragging technique can also be extensible applied to various type of tubular construct organs such as the esophagus, trachea, and intestine [53,54]. To increase the efficiency, functionality, and applicability of S-SDV, suitable natural polymers or growth factors can also be added through the multilayer design [55,56]. We propose the next step is to optimize the application *in vivo*, as the S-SDV is a promising approach for future clinical trials.

## CRedit authorship contribution statement

**Hun-Jin Jeong:** Project administration, Writing – original draft, Methodology, Investigation. **Hyoryung Nam:** Project administration, Writing – original draft, Methodology, Investigation. **Jae-Seok Kim:** Investigation, Validation. **Sungkeon Cho:** Investigation, Validation. **Hyun-Ha Park:** Resources, Funding acquisition. **Young-Sam Cho:** Methodology. **Hyungkook Jeon:** Software. **Jinah Jang:** Supervision, Conceptualization, Funding acquisition, Writing-Reviewing and Editing. **Seung-Jae Lee:** Supervision, Conceptualization, Funding acquisition, Writing-Reviewing and Editing.

## Declaration of competing interest

Hun-Jin Jeong, Hyoryung Nam, Young-Sam Cho, Jinah Jang, Seung-Jae Lee have competing interest since they are the inventor of a patent on the Artificial esophageal scaffold with multi-layer tubular using 3D bioprinting and fabricating device and fabricating method thereof (Korea Patent no. 10–2274151). Hun-Jin Jeong, Young-Sam Cho, Jinah Jang, Seung-Jae Lee have competing interest since they are the inventor of a patent on the Artificial vascular scaffold with multi-layer tubular using 3D bioprinting and fabricating device and fabricating method thereof (Korea Patent no. 10–2306282). Hun-Jin Jeong, Young-Sam Cho, Seung-Jae Lee have competing interest since they are the inventor of a patent on the Scaffold and fabrication method by dragging technique (Korea Patent no. 10–2026635). The remaining authors declare that they have no known competing financial interests or personal relationships that could have appeared to influence the work reported in this paper.

## Acknowledgment

This work was supported by the National Research Foundation of Korea (NRF) grant funded by the Korea government (MSIT) (No. 2022R1A2C2008149, 2021R1C1C1008767); the Korean Fund for Regenerative Medicine funded by Ministry of Science and ICT, and Ministry of Health and Welfare (21A0104L1, Republic of Korea); and Korea Health Technology R&D Project through the Korea Health Industry Development Institute (KHIDI), funded by the Ministry of Health & Welfare, Republic of Korea (HI21C110000021); and the Alchemist Project (20012378, Development of Meta Soft Organ Module Manufacturing Technology without Immunity Rejection and Module Assembly Robot System) funded by the Ministry of Trade, Industry & Energy (MOTIE, Korea).

## Appendix A. Supplementary data

Supplementary data to this article can be found online at <https://doi.org/10.1016/j.bioactmat.2023.07.021>.

## References

- S. Das, H. Nam, J. Jang, 3D bioprinting of stem cell-laden cardiac patch: a promising alternative for myocardial repair (in English), *Appl Bioeng* 5 (3) (Sep 1 2021). <https://doi.org/10.1016/j.apbioeng.2021.100633>.
- M. Thiriet, Cardiovascular disease: an introduction (in English), *Biomath Biomech Mode* 8 (2018) 1–90, [https://doi.org/10.1007/978-3-319-89315-0\\_1](https://doi.org/10.1007/978-3-319-89315-0_1).
- Tsao, "Heart disease and stroke statistics-2022 update: a report from the American heart association (vol 145, pg e153, 2022)," (in English), *Circulation* 146 (10) (Sep 6 2022), <https://doi.org/10.1161/Cir.0000000000001074>. E141–E141.
- R.V. Jensen, M.V. Hjortbak, H.E. Botker, Ischemic heart disease: an update (in English), *Semin. Nucl. Med.* 50 (3) (May 2020) 195–207, <https://doi.org/10.1053/j.semnuclmed.2020.02.007>.
- R. Hajar, Risk factors for coronary artery disease: historical perspectives, *Heart Views* 18 (3) (Jul-Sep 2017) 109–114, <https://doi.org/10.4103/HEARTVIEWS.HEARTVIEWS.106.17>.
- S. Mendis, et al., "World Health Organization definition of myocardial infarction: 2008-09 revision," (in English), *Int. J. Epidemiol.* 40 (1) (Feb 2011) 139–146, <https://doi.org/10.1093/ije/dyq165>.
- B.R. Pagliaro, F. Cannata, G.G. Stefanini, L. Bolognese, Myocardial ischemia and coronary disease in heart failure (in English), *Heart Fail. Rev.* 25 (1) (Jan 2020) 53–65, <https://doi.org/10.1007/s10741-019-09831-z>.
- P. Mallis, E. Michalopoulos, C. Stavropoulos-Giokas, Modern approaches in cardiovascular disease therapeutics: from molecular genetics to tissue engineering, *Bioengineering (Basel)* 8 (11) (Nov 4 2021), <https://doi.org/10.3390/bioengineering8110174>.
- P. Mallis, A. Kostakis, C. Stavropoulos-Giokas, E. Michalopoulos, Future perspectives in small-diameter vascular graft engineering, (in English), *Bioengineering-Basel* 7 (4) (Dec 2020). ARTN 16010.3390/bioengineering7040160.
- M.R. Hoenig, G.R. Campbell, B.E. Rolfe, J.H. Campbell, Tissue-engineered blood vessels: alternative to autologous grafts? *Arterioscler. Thromb. Vasc. Biol.* 25 (6) (Jun 2005) 1128–1134, <https://doi.org/10.1161/01.ATV.0000158996.03867.72>.
- G. Gao, et al., Tissue engineered bio-blood-vessels constructed using a tissue-specific bioink and 3D coaxial cell printing technique: a novel therapy for ischemic disease (in English), *Adv. Funct. Mater.* 27 (33) (Sep 6 2017). ARTN 170079810.1002/adfm.201700798.
- G. Gao, et al., Tissue-engineering of vascular grafts containing endothelium and smooth-muscle using triple-coaxial cell printing (in English), *Appl. Phys. Rev.* 6 (4) (Dec 2019). ARTN 04140210.1063/1.5099306.
- O. Goeau-Brissonniere, C. Lepout, F. Bacourt, C. Lebrault, R. Comte, J.C. Pechere, Prevention of vascular graft infection by rifampin bonding to a gelatin-sealed Dacron graft, *Ann. Vasc. Surg.* 5 (5) (Sep 1991) 408–412, <https://doi.org/10.1007/BF02133043>.
- P.C. Begovac, R.C. Thomson, J.L. Fisher, A. Hughson, A. Gallhagen, Improvements in GORE-TEX vascular graft performance by Carmeda BioActive surface heparin immobilization, *Eur. J. Vasc. Endovasc. Surg.* 25 (5) (May 2003) 432–437, <https://doi.org/10.1053/ejvs.2002.1909>.
- L. Xue, H.P. Greisler, "Biomaterials in the development and future of vascular grafts," (in English), *J. Vasc. Surg.* 37 (2) (Feb 2003) 472–480, <https://doi.org/10.1067/mva.2003.88>.
- M.A. Rodriguez-Soto, et al., Small diameter cell-free tissue-engineered vascular grafts: biomaterials and manufacture techniques to reach suitable mechanical properties (in English), *Polym. Bull. (Heidelberg, Ger.)* 14 (17) (Sep 2022). ARTN 344010.3390/polym14173440.
- S. Spadaccio, A. Rainer, R. Barbato, M. Trombetta, M. Chello, B. Meyns, The long-term follow-up of large-diameter Dacron (R) vascular grafts in surgical practice: a review (in English), *J. Cardiovasc. Surg.* 60 (4) (Aug 2019) 501–513, <https://doi.org/10.23736/S0021-9509.16.08061-7>.
- M.A. Hiob, S. She, L.D. Muiznieks, A.S. Weiss, Biomaterials and modifications in the development of small-diameter vascular grafts (in English), *ACS Biomater. Sci. Eng.* 3 (5) (May 2017) 712–723, <https://doi.org/10.1021/acsbomaterials.6b00220>.
- R. Zizhou, X. Wang, S. Houshyar, Review of polymeric biomimetic small-diameter vascular grafts to tackle intimal hyperplasia (in English), *ACS Omega* (Jun 21 2022), <https://doi.org/10.1021/acsomega.2c01740>.
- M. Zhou, et al., Development and validation of small-diameter vascular tissue from a decellularized scaffold coated with heparin and vascular endothelial growth factor (in English), *Artif. Organs* 33 (3) (Mar 2009) 230–239, <https://doi.org/10.1111/j.1525-1594.2009.00713.x>.
- X. Ma, et al., Development and in vivo validation of tissue-engineered, small-diameter vascular grafts from decellularized aortae of fetal pigs and canine vascular endothelial cells (in English), *J. Cardiothorac. Surg.* 12 (Nov 25 2017). ARTN 10110.1186/s13019-017-0661-x.
- G. Gao, J.Y. Park, B.S. Kim, J. Jang, D.W. Cho, Coaxial cell printing of freestanding, perfusable, and functional in vitro vascular models for recapitulation of native vascular endothelium pathophysiology, *Adv Healthc Mater* 7 (23) (Dec 2018), e1801102, <https://doi.org/10.1002/adhm.201801102>.
- S.Y. Hann, et al., Recent advances in 3D printing: vascular network for tissue and organ regeneration (in English), *Transl. Res.* 211 (Sep 2019) 46–63, <https://doi.org/10.1016/j.trsl.2019.04.002>.
- P.J. Wang, Y.Z. Sun, X.Q. Shi, H.X. Shen, H.H. Ning, H.T. Liu, 3D printing of tissue engineering scaffolds: a focus on vascular regeneration (in English), *Bio-Des Manuf* 4 (2) (Jun 2021) 344–378, <https://doi.org/10.1007/s42242-020-00109-0>.
- I. Holland, J. Logan, J. Shi, C. McCormick, D. Liu, W. Shu, 3D biofabrication for tubular tissue engineering, *Biodes Manuf* 1 (2) (2018) 89–100, <https://doi.org/10.1007/s42242-018-0013-2>.
- R. Wenger, M.N. Giraud, 3D printing applied to tissue engineered vascular grafts (in English), *Appl Sci-Basel* 8 (12) (Dec 2018). ARTN 263110.3390/ap.8122631.
- H. Tetsuka, S.R. Shin, "Materials and technical innovations in 3D printing in biomedical applications," (in English), *J. Mater. Chem. B* 8 (15) (Apr 21 2020) 2930–2950, <https://doi.org/10.1039/d0tb00034e>.
- X. Li, L. Liu, X. Zhang, T. Xu, Research and development of 3D printed vasculature constructs, *Biofabrication* 10 (3) (Apr 30 2018), 032002, <https://doi.org/10.1088/1758-5090/aab5d6>.
- H. Lee, T.S. Jang, G. Han, H.W. Kim, H.D. Jung, Freeform 3D printing of vascularized tissues: challenges and strategies, (in English), *J. Tissue Eng.* 12 (Nov 2021). ARTN 2041731421105723610.1177/20417314211057236.
- D. Chimene, R. Kaunas, A.K. Gaharwar, Hydrogel bioink reinforcement for additive manufacturing: a focused review of emerging strategies (in English), *Adv Mater* 32 (1) (Jan 2020). ARTN 190202610.1002/adma.201902026.
- H. Nam, et al., Multi-layered free-form 3D cell-printed tubular construct with decellularized inner and outer esophageal tissue-derived bioinks, *Sci. Rep.* 10 (1) (Apr 29 2020) 7255, <https://doi.org/10.1038/s41598-020-64049-6>.

- [32] M. Kobari, F. Gotoh, Y. Fukuuchi, K. Tanaka, N. Suzuki, D. Uematsu, Blood-flow velocity in the pial-arteries of cats, with particular reference to the vessel diameter (in English), *J Cerebr Blood F Met* 4 (1) (1984) 110–114, <https://doi.org/10.1038/jcbfm.1984.15>.
- [33] C. Magliaro, G. Mattei, F. Iacoangeli, A. Corti, V. Piemonte, A. Ahluwalia, Oxygen consumption characteristics in 3D constructs depend on cell density (in English), *Front. Bioeng. Biotechnol.* 7 (Oct 10 2019). ARTN 25110.3389/fbioe.2019.00251.
- [34] J.L. McReynolds, Modeling of an Oxygenation-Aided 3D Culture for Functional Beta-Cell Expansion, Biomedical Engineering Undergraduate Honors Theses, 2014. <https://scholarworks.uark.edu/bmeguht/5/>.
- [35] M.X. Li, et al., A biomimetic orthogonal-bilayer tubular scaffold for the co-culture of endothelial cells and smooth muscle cells, *RSC Adv.* 11 (50) (Sep 21 2021) 31783–31790, <https://doi.org/10.1039/d1ra04472a>.
- [36] S.G. Thomas, 3 - the structure of resting and activated platelets, *Platelets* (2019) 47–77, <https://doi.org/10.1016/B978-0-12-813456-6.00003-5> (Fourth Edition).
- [37] E. Carletti, A. Motta, C. Migliaresi, Scaffolds for tissue engineering and 3D cell culture, *Methods Mol. Biol.* 695 (2011) 17–39, [https://doi.org/10.1007/978-1-60761-984-0\\_2](https://doi.org/10.1007/978-1-60761-984-0_2).
- [38] I.M. Basurto, S.A. Muhammad, G.M. Gardner, G.J. Christ, S.R. Caliri, Controlling scaffold conductivity and pore size to direct myogenic cell alignment and differentiation, *J. Biomed. Mater. Res.* 110 (10) (Oct 2022) 1681–1694, <https://doi.org/10.1002/jbm.a.37418>.
- [39] H. Mehdizadeh, S. Sumo, E.S. Bayrak, E.M. Brey, A. Cinar, Three-dimensional modeling of angiogenesis in porous biomaterial scaffolds, *Biomaterials* 34 (12) (Apr 2013) 2875–2887, <https://doi.org/10.1016/j.biomaterials.2012.12.047>.
- [40] M.M. Nava, L. Draghi, C. Giordano, R. Pietrabissa, The effect of scaffold pore size in cartilage tissue engineering, in English, *J Appl Biomater Func* 14 (3) (Jul-Sep 2016) E223–E229, <https://doi.org/10.5301/jabfm.5000302>.
- [41] Q.L. Loh, C. Choong, Three-Dimensional scaffolds for tissue engineering applications: role of porosity and pore size (in English), *Tissue Eng. B Rev.* 19 (6) (Dec 1 2013) 485–502, <https://doi.org/10.1089/ten.teb.2012.0437>.
- [42] D.F. Wang, Y.Y. Xu, L.Q. Li, L.S. Turng, Artificial small-diameter blood vessels: materials, fabrication, surface modification, mechanical properties, and bioactive functionalities (in English), *J. Mater. Chem. B* 8 (9) (Mar 7 2020) 1801–1822, <https://doi.org/10.1039/c9tb01849b>.
- [43] W. Zhao, X. Jin, Y. Cong, Y.Y. Liu, J. Fu, Degradable natural polymer hydrogels for articular cartilage tissue engineering, in English, *J. Appl. Chem. Biotechnol.* 88 (3) (Mar 2013) 327–339, <https://doi.org/10.1002/jctb.3970>.
- [44] X.Y. Wang, V. Chan, P.R. Corridon, Acellular tissue-engineered vascular grafts from polymers: methods, achievements, characterization, and challenges (in English), *Polym. Bull. (Heidelberg, Ger.)* 14 (22) (Nov 2022). ARTN 482510.3390/polym14224825.
- [45] M.A. Cleary, E. Geiger, C. Grady, C. Best, Y. Naito, C. Breuer, Vascular tissue engineering: the next generation, in English, *Trends Mol. Med.* 18 (7) (Jul 2012) 394–404, <https://doi.org/10.1016/j.molmed.2012.04.013>.
- [46] A. Kruger-Genge, A. Blocki, R.P. Franke, F. Jung, Vascular endothelial cell biology: an update, *Int. J. Mol. Sci.* 20 (18) (Sep 7 2019), <https://doi.org/10.3390/ijms20184411>.
- [47] J. Heo, et al., Enhanced cellular distribution and infiltration in a wet electrospun three-dimensional fibrous scaffold using eccentric rotation-based hydrodynamic conditions, in English, *Sensor Actuat B-Chem* 226 (Apr 2016) 357–363, <https://doi.org/10.1016/j.snb.2015.11.030>.
- [48] G.A. Villalona, et al., Cell-seeding techniques in vascular tissue engineering, *Tissue Eng. B Rev.* 16 (3) (Jun 2010) 341–350, <https://doi.org/10.1089/ten.TEB.2009.0527>.
- [49] S. Bertlein, et al., Development of endothelial cell networks in 3D tissues by combination of melt electrospinning writing with cell-accumulation technology (in English), *Small* 14 (2) (Jan 11 2018). ARTN 170152110.1002/sml.201701521.
- [50] C. Michiels, T. Arnould, J. Remacle, Endothelial cell responses to hypoxia: initiation of a cascade of cellular interactions, *Biochim. Biophys. Acta* 1497 (1) (Jun 2 2000) 1–10, [https://doi.org/10.1016/S0167-4889\(00\)00041-0](https://doi.org/10.1016/S0167-4889(00)00041-0).
- [51] I. Baldea, et al., Effects of different hypoxia degrees on endothelial cell cultures—Time course study (in English), *Mech. Ageing Dev.* 172 (Jun 2018) 45–50, <https://doi.org/10.1016/j.mad.2017.11.003>.
- [52] J.W. Yau, H. Teoh, S. Verma, Endothelial cell control of thrombosis, *BMC Cardiovasc. Disord.* 15 (Oct 19 2015) 130, <https://doi.org/10.1186/s12872-015-0124-z>.
- [53] H.J. Jeong, H. Nam, J. Jang, S.J. Lee, 3D bioprinting strategies for the regeneration of functional tubular tissues and organs, *Bioengineering (Basel)* 7 (2) (Mar 31 2020), <https://doi.org/10.3390/bioengineering7020032>.
- [54] H. Han, et al., A bioprinted tubular intestine model using a colon-specific extracellular matrix bioink, in English, *Adv Healthc Mater* 11 (2) (Jan 2022). ARTN 210176810.1002/adhm.202101768.
- [55] H. Nam, et al., Multi-layered free-form 3D cell-printed tubular construct with decellularized inner and outer esophageal tissue-derived bioinks (in English), *Sci Rep-Uk* 10 (1) (Apr 29 2020). ARTN 725510.1038/s41598-020-64049-6.
- [56] J.Y. Park, G. Gao, J. Jang, D.W. Cho, 3D printed structures for delivery of biomolecules and cells: tissue repair and regeneration (in English), *J. Mater. Chem. B* 4 (47) (Dec 21 2016) 7521–7539, <https://doi.org/10.1039/c6tb01662f>.